Evidence of spin-polarized direct elastic tunneling and onset of superparamagnetism in MgO magnetic tunnel junctions

J. M. Teixeira,* J. Ventura, J. P. Araujo, and J. B. Sousa
IFIMUP and IN-Institute of Nanoscience and Nanotechnology, and Departamento de Fisica, Faculdade de Ciencias, Universidade do Porto, Rua do Campo Alegre, 687, 4169-007 Porto, Portugal

M. P. Fernández-García
Departamento de Fisica, Universidad de Oviedo, Calvo Sotelo, s/n, 33007 Oviedo, Spain

P. Wisniowski
Department of Electronics, AGH University of Science and Technology, 30-059 Krakow, Poland and INESC-MN, Rua Alves Redol, 9-1, 1000-029 Lisbon, Portugal

P. P. Freitas
INESC-MN and IN-Institute of Nanoscience and Nanotechnology, Rua Alves Redol, 9-1, 1000-029 Lisbon, Portugal
(Received 27 January 2010; revised manuscript received 15 March 2010; published 19 April 2010)

Magnetic tunnel junctions (MTJs) with crystalline MgO barriers are currently being used in a variety of applications, namely forefront magnetic sensors and memories. In this work we probed the temperature (T) dependence of the transport and magnetic properties of MgO-based MTJs with different CoFeB free layer thicknesses (t_{fl}=1.55, 1.65, 1.95, and 3.0 nm). All samples have the same insulating MgO barrier with a nominal thickness of 1.35 nm. Our results show that the tunnel magnetoresistance (TMR) temperature behavior is mainly due to a strong variation of the conductance (G) of the antiparallel state. Also, we provide evidence that direct elastic tunneling is the dominant mechanism determining the temperature dependence of the tunneling conductance and TMR in the studied MgO MTJs. Intrinsic to this mechanism is the thermal smearing of the electron energies near the Fermi level which then plays a key role in $G(T)$, especially in the parallel state where the overall change in G is very small. Furthermore, we show a clear change in the MTJ properties as the free layer thickness is reduced. Besides the typical decrease of TMR related with the loss of spin polarization, we were able to probe the thickness dependence of the spin wave α parameter. MTJ with the thinner free layer show both absence of hysteresis in the room temperature TMR cycles and interesting freezing effects in the zero and field cool magnetization curves at low temperatures, revealing the discontinuous nature of thin free layers.

DOI: 10.1103/PhysRevB.81.134423 PACS number(s): 85.30.Mn, 72.25.−b, 75.47.−m, 85.75.−d

I. INTRODUCTION

Magnetic tunnel junctions (MTJs) with crystalline MgO barriers have been extensively investigated due to the theoretically predicted and then experimentally verified giant tunnel magnetoresistance (TMR) effect.[1–4] In fact, huge room temperature (RT) TMR effects (604% and 1056%) were very recently reported in single[5] and double[6] MTJs. Beyond their fundamental physical interest, these systems have many potential applications, including magnetic random access memories (MRAMs) and various types of high-sensitivity field sensors, namely, forefront read heads.[7–9]

An important and still open research topic in MgO MTJs is the dependence on temperature (T) of the corresponding transport properties. The T dependence of the tunneling conductance (G) in MTJs (both with crystalline MgO or amorphous Al_2O_3 barriers) is weaker for parallel (P) than antiparallel (AP) alignment of the ferromagnetic (FM) electrodes.[3,4,10–12] Additionally, in MgO tunnel barriers the T variation of the parallel conductance (G_P) is much smaller than in Al_2O_3 barriers.[11] Therefore (even in systems with different FM electrodes)[12] the decrease in TMR with increasing temperature is mostly due to changes in the AP conductance (G_{AP}). Several mechanisms can be responsible for such an effect, including the thermal excitation of magnons in the FM electrodes, thermal excitation of magnetic impurities/defects in the barrier or at its interfaces and the thermal variation in the FM electronic structure. Different models were then developed to explain the TMR(T) dependence for the case of incoherent tunneling. One is the model of Shang *et al.*,[13] based on Julliere's model,[14] that takes into account both a T-dependent FM spin polarization (P) and spin-independent assisted tunneling. Another model, by Zhang *et al.*,[15] is based on two-dimensional spin waves excited by tunneling electrons at the insulator/FM interface. Further explanations include the excitation and absorption of phonons at the FM electrodes by tunneling electrons.[16] All these models were successfully applied to MTJs, not only with amorphous Al_2O_3 barriers,[10,13,17–19] but also with sputtered polycrystalline and epitaxial MgO barriers,[20–24] where coherent tunneling occurs.

Here we analyze the temperature dependencies (20–300 K) of G and TMR in sputtered CoFeB/MgO/CoFeB MTJs with varying CoFeB free layer thickness (t_{fl}=1.55, 1.65, 1.95, and 3.0 nm) but the same reference layer structure. All the samples have an insulating MgO barrier with a nominal

thickness of 1.35 nm. The conductance in the P state is found to be nearly T independent for all samples, while G_{AP} exhibits a monotonous and significant decrease with decreasing temperature in the MTJs with t_{fl}=1.95 and 3.0 nm. The samples with thinner CoFeB free layers (t_{fl}=1.55 and 1.65 nm) show a minimum in the $G(T)$ curve, leading to the appearance of a maximum in TMR(T). This behavior can be understood by the existence of discontinuous FM grains in such thin free layers which, below the corresponding blocking temperature (T_B), are difficult to align along the applied magnetic field, thus preventing full P/AP alignment between free and pinned layers.

We further show that spin-polarized direct elastic tunneling accounts for the above T dependencies, emerging as the dominant mechanism in our MgO-based MTJs. Intrinsic to this tunnel mechanism is the thermal smearing of the electron energies near the Fermi level (E_F),[25] usually disregarded as negligible. However, this effect can be discarded only when the changes in G are substantially higher due to other extrinsic phenomena (e.g., magnon- or phonon-assisted tunneling or hopping). This is not the case for MgO-based systems, particularly for the P state, where the overall conductance change is very small.

II. COHERENT TUNNELING AND TEMPERATURE DEPENDENT MODELS

A. Coherent tunneling and giant TMR

Spin dependent tunneling in epitaxial MgO-based MTJs has been well described by first-principles theory.[1,2] A single-crystal MgO barrier exhibits a spin filtering effect concerning the electron wave-function symmetry. For thick barriers and in the P state, tunneling is governed by the electronic Bloch states with Δ_1 symmetry (smaller spatial decay rate) and with momentum vectors normal to the barrier. The tunneling probability decreases very rapidly when the electron momentum vectors deviate from the barrier normal direction. On the other hand, the conductance in the AP configuration is very low, being related with the propagation of $\Delta_{5,2}$ states (large decay rates), resulting in giant TMR ratios. However, in thin barriers, electrons with momentum vectors deviating from the barrier normal direction have a finite tunneling probability and the contribution from $\Delta_{5,2}$ states becomes significant. The conductance in the AP state increases and TMR therefore decreases.

B. Temperature dependence of tunnel conductance and TMR

So far, first-principles theory cannot take into account the T dependence of the tunneling conductance and TMR ratio. However, several models were developed to explain the TMR(T) behavior for the case of amorphous barriers, including spin-polarized direct elastic tunneling, magnon- and phonon-assisted tunneling, hopping via localized states in the barrier and spin scattering at magnetic impurities. These models were also successfully applied to MgO MTJs.

In the model of Shang *et al.*[13] two tunneling contributions are considered. First, electron spin-polarized direct elastic tunneling between the FM electrodes, with a polarization P that decreases with T due to thermally excited spin waves according to $P(T)=P_0(1-\alpha T^{3/2})$, i.e., as the surface magnetization.[26] The parameter α is material-dependent and P_0 is the spin polarization at 0 K. The second contribution is related with spin-independent tunneling (G^{SI}), usually associated with hopping through localized states within the barrier. The total G is then written, following Julliere,[14] as

$$G(T) = G_T(1 + P_1P_2 \cos\ \theta) + G^{SI}, \tag{1}$$

where θ is the angle between the magnetizations of the two electrodes, G_T is the prefactor for direct elastic tunneling and P_1 and P_2 the FM electrodes polarization. Considering only the first term in Eq. (1), G_{AP} increases with T, which is the usual behavior observed in MTJs when spin-dependent tunneling dominates. Such increase comes essentially from the decrease of the spin polarization (P_1 and P_2), but also from the increase of G_T due to the broadening of the Fermi distributions in the electrodes. Theory gives $G_T=G(0) \times CT/\sin(CT)$,[27] where $G(0)$ is the zero temperature conductance and $C=1.387\times10^{-4}t/\sqrt{\phi}$, with the barrier thickness (t) in Å and the barrier height ϕ in eV.

Another possible mechanism that could contribute to $G(T)$ is the scattering of electrons by transition metal oxide interfacial impurities created at the FM/barrier interface. Usually, such impurities are of paramagnetic nature close to RT, where a stronger spin scattering should be expected, and antiferromagnetic at lower temperatures, where spin scattering should be greatly reduced.[28] Thus, a decrease in G is expected with increasing temperature.

The decrease in $\Delta G(T)$ ($=G_P-G_{AP}$) and TMR(T) with increasing temperature was predicted considering the excitation of magnons at the FM/insulator interface.[15] This behavior is the result of the spin-flip nature of the process that scatters the tunnel electron from majority to minority states, and vice versa, in the case of P alignment. On the contrary, for AP electrode alignment the electrons are scattered to states of the same spin sub-band in the two MTJ electrodes. An inelastic spin-conserving contribution to $G(T)$ is also sometimes needed to account for experimental results. A possible mechanism concerns the excitation and absorption of phonons at the metallic electrodes by tunneling electrons.[16] The theory predicts a $G_{P,AP}$ and ΔG increase with temperature. However, TMR(T) should decrease with T, since $G_{AP}(T)$ increases faster than ΔG.

III. EXPERIMENTAL DETAILS

A set of magnetic tunnel junctions was deposited in a Nordiko 2000 magnetron sputtering system with base pressure of 7×10^{-9} Torr in dc and rf (CoFe and MgO) modes. The complete structure of the deposited MTJs was Glass/Ta 5 nm/Ru 18 nm/Ta 3 nm/MnPt 16 nm/CoFe 2.2 nm/Ru 0.96 nm/CoFeB 3 nm/MgO 1.35 nm)/CoFeB (t)/Ru 5 nm/Ta 5 nm, where CoFe, CoFeB, and MnPt stand for $Co_{82}Fe_{18}$, $(Co_{52}Fe_{48})_{75}B_{25}$, and $Mn_{54}Pt_{46}$. The CoFeB free layer thickness was varied, with t_{fl}=1.55, 1.65, 1.95, and 3.0 nm. The MgO layer was grown out of a single crystal MgO target at 20 mTorr, 3 W/cm^2 and at a sample to target separation of 5 cm. For the other layers, typical deposition pressures were

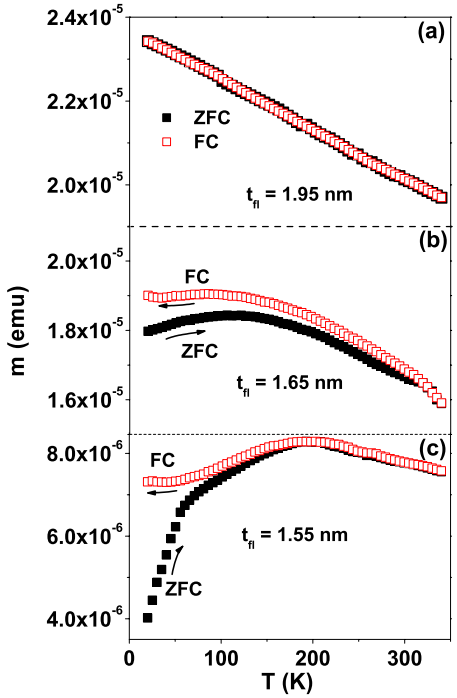

FIG. 1. (Color online) Zero-field-cooling (ZFC) and field-cooling (FC) magnetic moment (m) measurements, for the MTJs with (a) t_{fl}=1.95 nm; (b) 1.65 nm and (c) t_{fl}=1.55 nm.

from 2 to 4 mTorr, and typical power densities were 13 W/cm^2 at a sample to target separation of 10 cm. During deposition an in-plane magnetic field (H) of 20 Oe was applied to define the magnetic anisotropy axes of the pinned and free layers in the same direction. Before the patterning process, the structure was covered with 15 nm of $Ti_{10}W_{90}(N_2)$, also deposited by magnetron sputtering. MTJs were then microfabricated by optical lithography and ion beam milling in a rectangular shape with areas ranging between 1×1 and 5×6 μm^2. Patterned samples were annealed in high vacuum at 613 K, for 1 h in a magnetic field (H) of 5 kOe applied along the easy axis, and furnace cooled. Thermal annealing was used to improve the crystallinity (and reduce the number of defects and/or dislocations) of the MTJ. Note that the CoFeB layers, which are amorphous in the as-deposited state, become crystallized upon annealing.[29]

Transport properties were measured with a four-probe dc method with current stable to $1:10^6$ and using an automatic control and data acquisition system. Temperature-dependent measurements were performed in a closed cycle cryostat down to 20 K. Magnetic measurements were carried out with a superconducting quantum interference device (SQUID) magnetometer in RSO (Reciprocating Sample Oscillation) mode, between 20 and 340 K.

IV. EXPERIMENTAL RESULTS

A. Magnetic properties

Figure 1 illustrates the T dependence of the magnetic moment $[m(T)]$ of unpatterned MTJs with t_{fl} of 1.55, 1.65, and 1.95 nm in the zero-field-cooling (ZFC) and field-cooling (FC) regimes. In the ZFC process the samples were cooled from 340 K down to 20 K under H=0. A magnetic field of 50 Oe was then applied and the $m^{ZFC}(T)$ curve was measured on heating (20–340 K). On the other hand, the $m^{FC}(T)$ curve was measured under H=50 Oe while cooling the sample. One notes that the probing H favored the P state. The thicker samples (t_{fl}=1.95 and 3.0 nm; the last not shown) display FM ordering with $m^{ZFC}(T)$ and $m^{FC}(T)$ overlapping in the whole measured temperature range [Fig. 1(a)]. On the other hand, the MTJ with t_{fl}=1.65 nm displays a splitting between the $m^{ZFC}(T)$ and $m^{FC}(T)$ curves below ~320 K [Fig. 1(b)]. Finally, the $m^{ZFC}(T)$ and $m^{FC}(T)$ curves of the MTJ with t_{fl} =1.55 nm overlap above ~200 K [Fig. 1(c)], but a splitting is visible below such temperature.

These irreversibilities are similar to those observed in magnetically blocked nanoparticles.[30–35] For a system of nanoparticles, the superparamagnetic (SPM) behavior is well established when: (i) the $m^{ZFC}(T)$ curve displays a maximum at a certain temperature, known as the blocking temperature, T_B; (ii) the $m^{ZFC}(T)$ and $m^{FC}(T)$ curves overlap above T_B; (iii) for $T>T_B$, $M(H)$ cycles do not show coercivity nor remanence and follow the Langevin function. The above considerations are all fulfilled for the case of t_{fl}=1.55 nm (see also below), demonstrating the discontinuous nature of the thin CoFeB free layer. The broad maximum seen at ~200 K in the $m^{ZFC}(T)$ curve evidences the existence of a T_B distribution, related with a distribution of CoFeB grain sizes. A more exhaustive analysis of the $m^{ZFC}(T)$ curve can be performed using the Stoner-Wohlfarth expression[36] for $m^{ZFC}(T)$ under low applied magnetic fields (for details see Ref. 31),

$$\chi^{ZFC} = \lim_{H\to 0}\frac{M^{ZFC}}{H} = \frac{\mu_0 M_S^2}{3K\rho}\left[\frac{E_{bm}}{k_B T}\int_0^{T/T_{Bm}} yf(y)dy + \int_{T/T_{Bm}}^{\infty} f(y)dy\right], \quad (2)$$

where the size distribution of the nanoparticles is described by a log-normal distribution,

$$f(y)dy = \frac{A}{\sqrt{2\pi}\sigma y}\exp\left(-\frac{ln^2 y}{2\sigma^2}\right)dy. \quad (3)$$

The first term in Eq. (2) corresponds to the SPM contribution of the nanoparticles and the second to the nanoparticles in the blocked state. Figure 2 shows the successful fit of the $m^{ZFC}(T)$ curve with Eq. (2). Using the values of CoFeB for the anisotropy constant,[37] K=19 900 erg cm^{-3}, density[37] ρ=7.8 g cm^{-3} and saturation magnetization[38] M_S =860 emu cm^{-3}, we obtain an average diameter $\langle D\rangle$ $\simeq$46 nm for the CoFeB grains. Such value is in good agreement with recent results published by Shen *et al.*[39] on MgO-based MTJs with similar CoFeB free layers thicknesses. The grain dimension obtained from the ZFC fit imply a pancake-like shape for the CoFeB particles, since it is much higher than the nominal thickness of the FM free layer (1.55 nm). Finally, the inset of Fig. 2 displays a normalized TMR(H) curve at T=300 K, showing the virtual absence of hysteresis. The good fit of TMR(H) with a Langevin function[39]

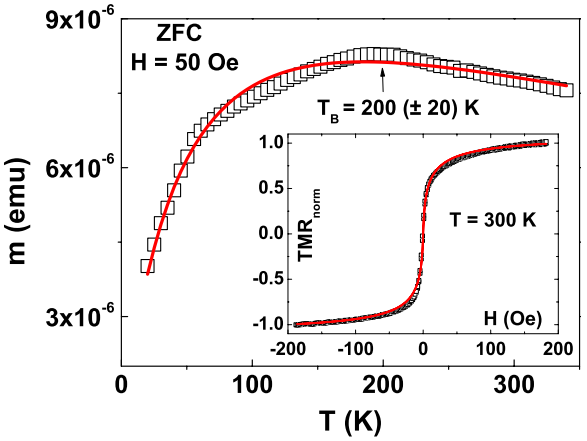

FIG. 2. (Color online) ZFC magnetic moment measurements in the 20–340 K range for the MTJ with t_{fl}=1.55 nm. Inset: normalized TMR(H) curve of the same MTJ at 300 K. Solid lines are fits using Eq. (2) for $m^{ZFC}(T)$ and the Langevin function for TMR(H).

confirms the discontinuous (granular) nature of the FM free layer in this MTJ, with a T_B below 300 K.

Although the MTJ with t_{fl}=1.65 nm [Fig. 1(b)] also displays features characteristic of a system of blocked nanoparticles, the $m^{ZFC}(T)$ curve could not be fitted by the above model. However, the observed higher overlapping temperature (~320 K) still suggests the presence of discontinuous grains, but larger than those of the MTJ with t_{fl}=1.55 nm.

B. Transport properties

The TMR(H) [=$G_P/G(H)-1$] loops of the studied MTJs (t_{fl} from 1.55 to 3.0 nm), measured at low bias voltage (~5 mV) and different temperatures (20–300 K), are illustrated in Fig. 3. The loops were obtained by sweeping the field within the limits ±200 Oe and always along the easy magnetic axis. For the MTJs with thicker CoFeB free layers [t_{fl}=3.0 and 1.95 nm; Figs. 3(a) and 3(b)], one sees an increase of TMR from 165% to 223% and from 132% to 214%, between RT and 20 K; also, the TMR(H) loops exhibit a significant squareness. Such squareness is rapidly lost as one goes to t_{fl}=1.65 and 1.55 nm [Figs. 3(c) and 3(d)]. In the later case, the TMR(H) results confirm the SPM behavior observed in $M(T)$, with no coercive field (H_c) near RT, i.e., hysteresis-free switching. For $T<225$ K hysteresis starts to appear, greatly increasing as T decreases. The particular case of t_{fl}=1.65 nm, for which hysteresis is seen over the 20–300 K range but the ZFC and FC curves overlap above RT, will be discussed in more detail below. Finally, for t_{fl} >1.65 nm, long-range order percolation takes over: granule coalescence spreads as t_{fl} increases, toward a continuous magnetic free layer.

Another interesting effect seen in TMR(H) for the t_{fl} =1.55 nm sample is the nonsaturation of the TMR curve for the maximum applied magnetic field (200 Oe) and T ≤200 K [Fig. 3(d)]. This indicates a lack of full antiparallelism between free and pinned layers, which increases as T decreases. Also present, but less noticeable, is the nonsaturation of the P state below 200 K (H=−200 Oe). A similar

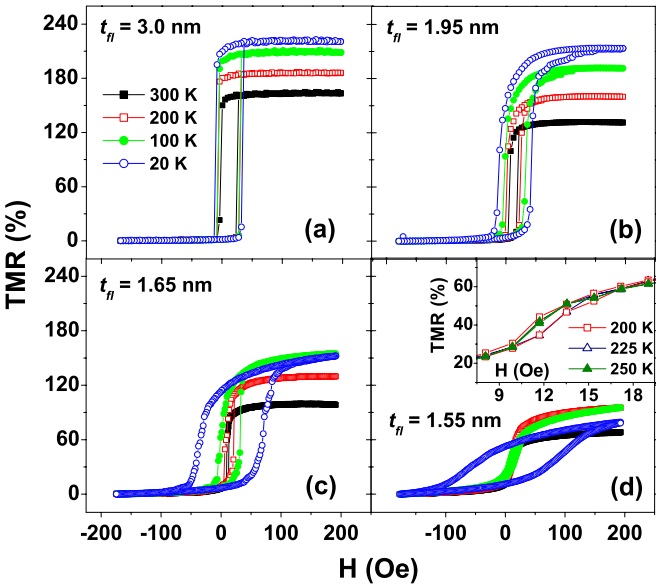

FIG. 3. (Color online) Representative TMR(H) curves between 20 and 300 K for MTJs with free layer thicknesses of (a) 3.0 nm, (b) 1.95 nm, (c) 1.65 nm and (d) 1.55 nm. Note the evolution of the TMR ratio with t_{fl}. Inset in (d): zoom of TMR(H) at T=200, 225 and 250 K, for t_{fl}=1.55 nm; note the absence of hysteresis for T ≥225 K.

(although smaller) effect is visible in the low temperature TMR(H) curves of the t_{fl}=1.65 nm sample [Fig. 3(c)]. Such effect will be relevant for the physical explanation of the $G(T)$ behavior, as detailed below. We also see important changes in the TMR magnitude as t_{fl} decreases: for t_{fl} =1.65 nm we have TMR=99% at RT and 152% at 20 K; for t_{fl}=1.55 nm, TMR=69% at RT, with only a slight increase to 79% at 20 K. This change in TMR with t_{fl} (Refs. 10, 39, and 40) indicates a significant weakening of FM order in the free layer as t_{fl} decreases to very thin values.

Figure 4 displays the $H_c(T)$ behavior of the free layer for all MTJs, showing that the variation in coercivity with temperature is much larger in the thinner samples (t_{fl}=1.55 and 1.65 nm). Returning to the squareness of the TMR(H) loops, we observe (inset of Fig. 4) that the $S(T)$ values of the (two) thicker free layer samples remain fairly constant over the whole temperature range (S≃0.90 and 0.70); this behavior is typical of MTJs with FM layers. Smaller values of S (≃0.63 at 20 K and 0.33 at RT) and a smooth increase with decreasing T are observed for the sample with t_{fl}=1.65 nm. On the other hand, the sample with t_{fl}=1.55 nm exhibits S values close to zero for T≥225 K [TMR(H) hysteresis-free switching] and a significant increase below 100 K (with S=0.47 at 20 K), accompanied by the rapid increase of H_c at low temperatures. Our transport results clearly indicate the presence of a state of magnetically blocked particles (discontinuous grains) at low T and SPM-like behavior near RT for the MTJ with t_{fl}=1.55 nm. In this case the value of T_B~200 K extracted from the magnetic measurements agrees well with the appearance of coercivity in the TMR(H) loops.

Figure 5 shows the zero-bias $G(T)$ dependence, in both magnetic states, for the studied MTJs. Judging from the form of the $G(T)$ curves, where an overall increase of $G_{P,AP}$ with

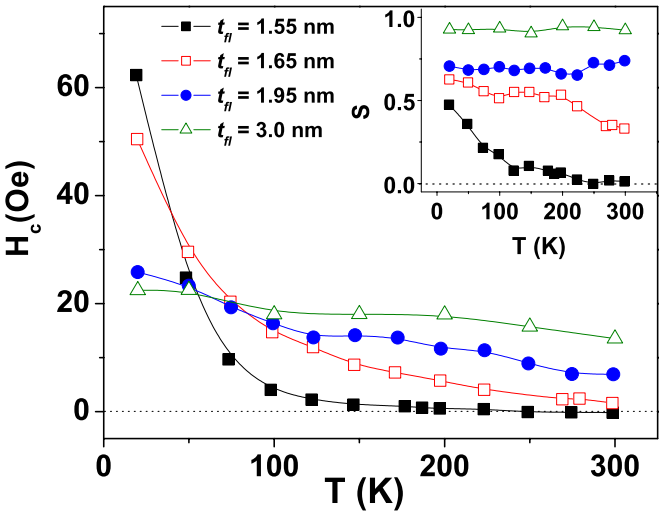

FIG. 4. (Color online) Coercive field of the free layer as a function of temperature for the studied MTJs. The inset graph shows the T-dependence of the squareness (S) of the loops, here defined as $S=(G_{AP}/G_{H\ coupl})[(G_m-G_{H\ coupl})/(G_m-G_{AP})]$, where $G_m=(2G_P G_{AP})/(G_P+G_{AP})$ and $G_{H\ coupl}$ is the conductance at the coupling field between pinned and free layers.

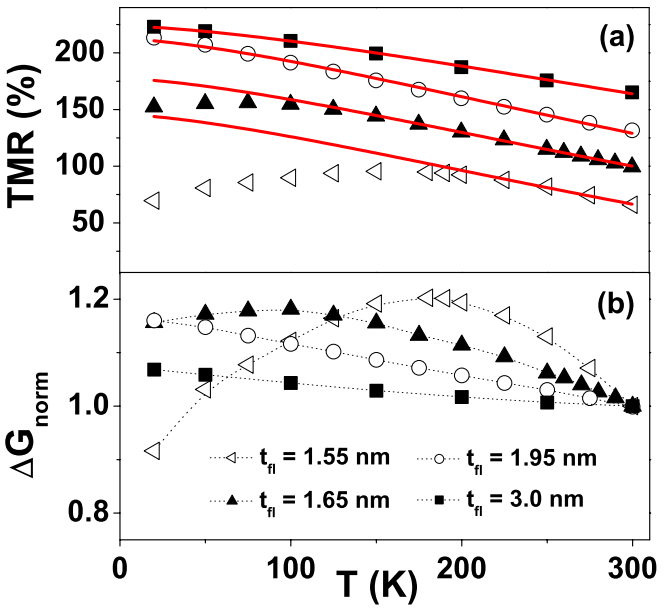

FIG. 6. (Color online) Temperature dependence of (a) TMR and (b) ΔG ($=G_P-G_{AP}$) for the studied MTJs. Solid lines are fits to the experimental databased on spin-polarized direct elastic tunneling model.

increasing T is observed (for the low T anomaly of the MTJ with t_{fl}=1.55 nm, see below), we exclude the existence of metallic pinholes across the barrier.[41–43] Furthermore, G_P increases only slightly on our MgO-based MTJs, a characteristic feature of high quality MgO tunneling barriers.[20–23]

V. DISCUSSION

Our experimental $G(T)$ and TMR(T) data were fitted using the spin-polarized direct elastic tunneling model, described by the first term of Eq. (1). The solid lines in Figs. 5 and 6(a) correspond to such fittings. In total there are four

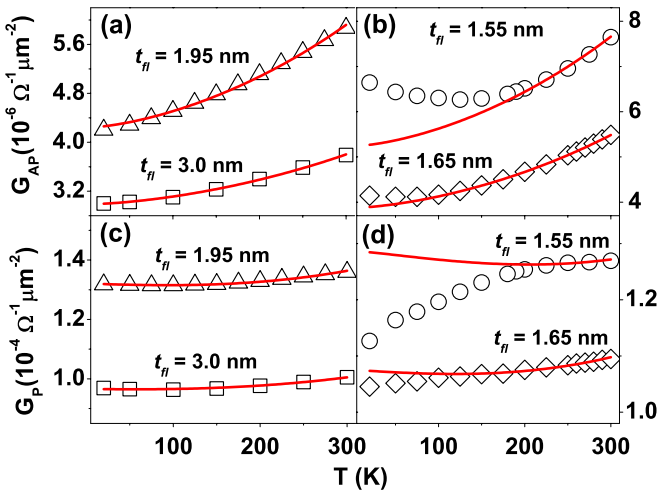

FIG. 5. (Color online) Temperature dependence of G in AP (a), (b) and P (c), (d) states for the studied MTJs, under an applied field $H=\pm 200$ Oe, respectively. The solid lines are fits to the experimental databased on the spin-polarized direct elastic tunneling model [first term of Eq. (1)].

adjustable parameters: P_0, α, G_0, and C to fit the $G_{P,AP}(T)$ and TMR(T) curves. The parameters P_0 and α are determined by fitting the TMR(T) curves, while G_0 and C are obtained from the $G_{P,AP}(T)$ data. The P_0 and α values of the pinned layer are determined by the fit of the transport curves of the MTJ with t_{fl}=3.0 nm, and assumed the same for all other samples. As illustrated in Figs. 5 and 6(a), the fits reproduce the experimental data quite well for the MTJs with t_{fl}=3.0 and 1.95 nm.

However, the $G_{P,AP}(T)$ and TMR(T) curves of the thinner samples (t_{fl}=1.55 and 1.65 nm) cannot be fitted over the whole 20–300 K range, due to the imperfect alignment of the free and pinned layer magnetizations observed at low T [cos θ term in Eq. (1)]. Thus, the P and AP states are not fully realized over the whole temperature range. Using the parameters obtained from the fits and the experimental $G(T)$ curves, we calculate $\theta\sim 128°$ (157°) at H=+200 Oe, AP-like state, and 20 K, for t_{fl}=1.55 nm (1.65 nm). As mentioned, the CoFeB free layers with thicknesses in the 1.55–1.65 nm range exhibit SPM-like or very weak FM order near RT, and blocked behavior at low T. Our transport results can then be explained as follows: in the SPM-like state, the magnetic moments of the free layer can be aligned by the external field, but at low T, with the onset of the blocked state, an increasing number of magnetic grains will be frozen in directions different from that of the induced uniaxial anisotropy (and thus of the applied field). This results in an imperfect alignment of the free and pinned layer magnetizations due to insufficient magnetic field.

The MTJ with t_{fl}=1.65 nm is characterized by a very small hysteresis at RT ($H_c\simeq 2$ Oe; Fig. 3). Since the free layer is only slightly thicker than 1.55 nm, we also expect the presence of magnetically inhomogeneous regions, likely constituted by large but still discontinuous grains. This is con-

TABLE I. The fitting parameters for the tunnel $G_{P,AP}(T)$ and TMR(T) curves of the studied MTJs to the model of spin-polarized direct elastic tunneling.

t_{fl} (nm)	1.55	1.65	1.95	3.0
P_0 (%)	58 ± 1	65 ± 0.1	71 ± 0.1	73 ± 0.04
α (10^{-5} $K^{-3/2}$)	6.9 ± 0.4	4.5 ± 0.05	3.4 ± 0.09	1.5 ± 0.02
$G^P(0)$ ($10^{-4}\Omega^{-1}$)	1.7 ± 0.02	0.7 ± 0.0006	26.1 ± 0.02	3.8 ± 0.005
$G^{AP}(0)$ ($10^{-4}\Omega^{-1}$)	1.7 ± 0.02	0.7 ± 0.0006	26.2 ± 0.09	3.8 ± 0.007
C^P (10^{-3} K^{-1})	2.8 ± 0.1	2.8 ± 0.01	2.8 ± 0.02	2.5 ± 0.03
C^{AP} (10^{-3} K^{-1})	2.8 ± 0.1	2.8 ± 0.01	2.7 ± 0.08	2.4 ± 0.04

firmed by the overlapping of the ZFC/FC curves above RT [~320 K; Fig. 1(b)], the large decrease of the coercivity with increasing temperature, almost reaching zero at RT, and by the behavior of the squareness of the TMR(H) loops (Fig. 3 and inset). Again the cos θ term in Eq. (1) can account for the observed $\Delta G(T)$ and TMR(T) deviations from the fit at low temperature.

Table I displays the fitting parameters obtained for the studied samples. One sees that P_0 decreases with t_{fl} by ~20% from the thicker to the thinner sample, as illustrated in Fig. 7. This decrease is related with the weakening of the FM order from 3.0 to 1.55 nm, as evidenced by our magnetic and transport results. Moreover, P_0 is sensitive to disorder and defects in the FM electrodes and at the FM/insulator interface. In our case, the small thickness of the CoFeB layers results in a structure of discontinuous grains, having pancakelike shape, as explained in Sec. IV A. On the other hand, we see that α increases with decreasing free layer thickness (Fig. 7). The values found are of the same order of magnitude of those found for most metals and alloys in thin films.[10,13] It is known that the spin wave α parameter is generally larger at the surface than in the bulk, due to surface exchange softening.[44] It has also been observed to be very sensitive to chemical interfaces, roughness and magnetic anisotropy.[45,46] Even in dot arrays, α was found to be larger than in the corresponding continuous film.[47] Our results thus indicate the sensitivity of α to magnetic inhomogeneous distribution of local spins, caused by material disorder or discontinuity at the interface between free and insulating layers.

The C parameter, related with the thickness and height of the barrier, is, as expected, approximately constant since all the MTJs have the same 1.35 nm MgO thickness. From the obtained C values we estimate a barrier height ϕ between 0.45–0.59 eV, which is consistent with theoretical calculations[1] and other experimental results.[3,4,24,48] Since this parameter appears in the broadening of the Fermi distribution of the electrodes, one defines the quantity $\beta=[C\times 300\ \text{K}/\sin(C\times 300\ \text{K})-1]$, to indicate the conductance variation due to this effect over the 0–300 K range. We find $\beta \simeq 12\%$, so that this phenomenon cannot be ignored in our MTJs, particularly for the P state where the overall $G(T)$ change is very small. Furthermore, for the P state, G_T and the polarization will contribute with opposite slopes to the T dependence of the overall conductance, and the small $G_P(T)$ dependence can be explained by a thermal competition between these two contrary effects. The importance of thermal smearing in MgO-based MTJs was also recently reported.[22] Evidence of the interesting competition between thermal smearing and polarization can be observed in Ref. 24, in which an unusually small $G_P(T)$ decrease with increasing T is reported for epitaxial Fe/MgO/Fe MTJs with $t_{MgO}=2.1$ and 1.5 nm, together with a T-independent G_P for $t_{MgO}=3.0$ nm. They have estimated $\phi=0.60$ eV, for which one finds β up to $\simeq 61\%$, again showing the importance of thermal smearing. One should now address why were good fits obtained using only the spin-polarized direct elastic tunneling model.

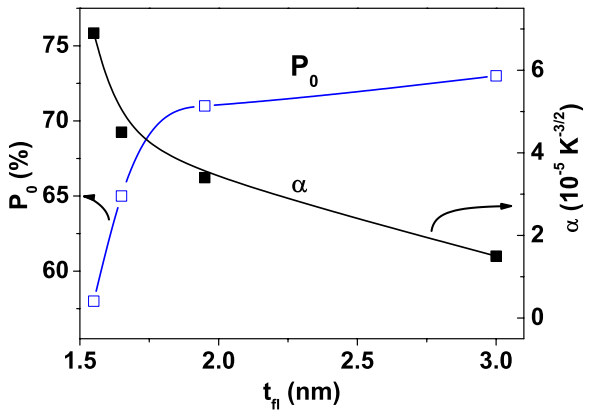

FIG. 7. (Color online) Spin polarization at 0 K and α parameter as a function of free layer thickness.

(i) A hopping mechanism [G_{SI} term in Eq. (1)] including at least two localized states inside the barrier should be negligible for the crystalline MTJs under study. First because multiple step hopping, although demonstrating itself in thick barriers ($t \gg 1$ nm), is not operative in thin barriers, where one-step tunneling is favored due to the exponential decrease of the tunnel probability with the barrier thickness.[49,50] The MgO thickness (1.35 nm) of our MTJs is far from such thick barrier regime. Also, a hopping mechanism cannot account for the T dependence of ΔG in the studied MTJs [Fig. 7(a)]. Such dependence also excludes assisted tunneling by magnetic impurities in the barrier.[51]

(ii) Although magnon-assisted tunneling is qualitatively consistent with the experimental trends in the MTJs with $t_{fl}=1.95$ and 3.0 nm, the fits to the corresponding theoretical model give unphysical values. Besides, magnon-assisted tunneling is an inelastic, higher order process with a tunneling matrix element much smaller than for spin-polarized direct elastic tunneling.[15,17]

(iii) Finally, phonon-assisted tunneling from the FM electrodes should lead to a systematic ΔG increase with T. Such trend appears only at low T in the two thinner MTJs [Fig.

6(b)]. The other (thicker) MTJs display a systematic ΔG increase from 20 to 300 K. Since our samples only differ on the FM free layer thickness, having the same MgO barrier, such ΔG differences at low T cannot be due to an inelastic spin-conserving contribution, and were convincingly explained by a lack of full parallelism/antiparallelism due to frozen grains below T_B. Therefore, spin-polarized direct elastic tunneling is the most suitable mechanism to describe the $G(T)$ and TMR(T) dependencies in the studied MTJs, as confirmed by the successful fit of our experimental data.

VI. CONCLUSIONS

In summary, spin-polarized direct elastic tunneling in thin MgO-based MTJs with different CoFeB free layer thicknesses was evidenced as the dominant tunneling mechanism. Various contributions to the tunnel G were discussed using different models, but the direct elastic tunneling plays the crucial role in determining the T-dependent behavior of G and TMR. This mechanism was successfully used to fit the experimental data with a good quantitative explanation of the experimental results. Our work has also shown that thermal smearing of the tunnel electron energy plays a key role in the $G(T)$ behavior of MgO-based MTJs, especially in the P state where the overall change in G_P with T is very small. This effect can be ignored only when changes in the tunnel G are substantially higher due to other extrinsic effects. Our transport and magnetic results also indicate the presence of discontinuous grains in the free layer for small enough thicknesses, leading to interesting freezing effects.

ACKNOWLEDGMENTS

This work was supported in part by Grants No. FEDERPOCTI/0155 and No. PTDC/CTM/73263/2006 from FCT and Projects No. IST-2001-37334 NEXT MRAM and NANO/NMED-SD/0140/2007. The authors acknowledge funding from FCT through the Associated Laboratory-IN. J.M.T. is thankful for an FCT grant (Grant No. SFRH/BD/24012/2005). M.P.F. thanks MICINN for the award of a FPI grant cofinanced by the European Social Fund. P.W. acknowledges the financial support provided through the European Community's Marie Curie Actions (Research Training Networks) under Contract No. MRTN-CT-2003-504462 (ULTRASMOOTH). J.V. acknowledges financial support through FSE/POPH.

*jmteixeira@fc.up.pt

[1] W. H. Butler, X.-G. Zhang, T. C. Schulthess, and J. M. MacLaren, Phys. Rev. B **63**, 054416 (2001).
[2] J. Mathon and A. Umerski, Phys. Rev. B **63**, 220403(R) (2001).
[3] S. S. P. Parkin, C. Kaiser, A. Panchula, P. M. Rice, B. Hughes, M. Samant, and See-Hun Yang, Nature Mater. **3**, 862 (2004).
[4] S. Yuasa, T. Nagahama, A. Fukushima, Y. Suzuki, and K. Ando, Nature Mater. **3**, 868 (2004).
[5] S. Ikeda, J. Hayakawa, Y. Ashizawa, Y. M. Lee, K. Miura, H. Hasegawa, M. Tsunoda, F. Matsukura, and H. Ohno, Appl. Phys. Lett. **93**, 082508 (2008).
[6] L. X. Jiang, H. Naganuma, M. Oogane, and Y. Ando, Appl. Phys. Express **2**, 083002 (2009).
[7] J.-G. Zhu and C. Park, Mater. Today **9**, 36 (2006).
[8] R. W. Dave, G. Steiner, J. M. Slaughter, J. J. Sun, B. Craigo, S. Pietambaram, K. Smith, G. Grynkewich, M. DeHerrera, J. Akerman, and S. Tehrani, IEEE Trans. Magn. **42**, 1935 (2006).
[9] O. G. Heinonen, E. W. Singleton, B. W. Karr, Z. Gao, H. S. Cho, and Y. H. Chen, IEEE Trans. Magn. **44**, 2465 (2008).
[10] L. Yuan, S. H. Liou, and D. Wang, Phys. Rev. B **73**, 134403 (2006).
[11] S. Parkin, H. Yang, S.-H. Yang, and M. Hayashi, *Handbook of Magnetism and Advanced Magnetic Materials* (Wiley, New York, 2007), Vol. 5.
[12] T. Ishikawa, T. Marukame, H. Kijima, K.-I. Matsuda, T. Uemura, M. Arita, and M. Yamamoto, Appl. Phys. Lett. **89**, 192505 (2006).
[13] C. H. Shang, J. Nowak, R. Jansen, and J. S. Moodera, Phys. Rev. B **58**, R2917 (1998).
[14] M. Julliere, Phys. Lett. **54A**, 225 (1975).
[15] S. Zhang, P. M. Levy, A. C. Marley, and S. S. P. Parkin, Phys. Rev. Lett. **79**, 3744 (1997).
[16] A. M. Bratkovsky, Appl. Phys. Lett. **72**, 2334 (1998).
[17] X.-F. Han, A. C. C. Yu, M. Oogane, J. Murai, T. Daibou, and T. Miyazaki, Phys. Rev. B **63**, 224404 (2001).
[18] T. Dimopoulos, Y. Henry, V. D. Costa, C. Tiusan, and K. Ounadjela, J. Appl. Phys. **95**, 6936 (2004).
[19] J. Schmalhorst, A. Thomas, S. Kammerer, O. Schebaum, D. Ebke, M. D. Sacher, G. Reiss, A. Hutten, A. Turchanin, A. Golzhauser, and E. Arenholz, Phys. Rev. B **75**, 014403 (2007).
[20] X. Kou, J. Schmalhorst, A. Thomas, and G. Reissa, Appl. Phys. Lett. **88**, 212115 (2006).
[21] X. Y. Liu, D. Mazumdar, W. F. Shen, B. D. Schrag, and G. Xiao, Appl. Phys. Lett. **89**, 023504 (2006).
[22] V. Drewello, J. Schmalhorst, A. Thomas, and G. Reiss, Phys. Rev. B **77**, 014440 (2008).
[23] S. G. Wang, R. C. C. Ward, G. X. Du, X. F. Han, C. Wang, and A. Kohn, Phys. Rev. B **78**, 180411(R) (2008).
[24] Q. L. Ma, S. G. Wang, J. Zhang, Yan Wang, R. C. C. Ward, C. Wang, A. Kohn, X.-G. Zhang, and X. F. Han, Appl. Phys. Lett. **95**, 052506 (2009).
[25] J. J. Akerman, I. V. Roshchin, J. M. Slaughter, R. W. Dave, and I. K. Schuller, Europhys. Lett. **63**, 104 (2003).
[26] A. H. MacDonald, T. Jungwirth, and M. Kasner, Phys. Rev. Lett. **81**, 705 (1998).
[27] J. G. Simmons, J. Appl. Phys. **35**, 2655 (1964).
[28] J. S. Moodera, J. Nowak, and R. J. M. van de Veerdonk, Phys. Rev. Lett. **80**, 2941 (1998).
[29] J. M. Teixeira, R. F. A. Silva, J. Ventura, A. M. Pereira, F. Carpinteiro, J. P. Araujo, J. B. Sousa, S. Cardoso, R. Ferreira, and P. P. Freitas, Mater. Sci. Eng., B **126**, 180 (2006).
[30] J. L. Dormann and D. Fiorani, *Magnetic Properties of Fine Particles* (North-Holland, Amsterdam, 1992).
[31] F. Bødker, M. F. Hansen, C. B. Koch, K. Lefmann, and S.

Mørup, Phys. Rev. B **61**, 6826 (2000).
[32] P. Gorria, M. P. Fernández, M. Sevilla, J. A. Blanco, and A. B. Fuertes, Phys. Status Solidi (RRL) **3**, 4 (2009).
[33] M. P. Fernández, D. S. Schmool, A. S. Silva, M. Sevilla, A. B. Fuertes, P. Gorria, and J. A. Blanco, J. Non-Cryst. Solids **354**, 5219 (2008).
[34] S. Bedanta and W. Kleemann, J. Phys. D **42**, 013001 (2009).
[35] M. P. Fernández-García, P. Gorria, J. A. Blanco, A. B. Fuertes, M. Sevilla, R. Boada, J. Chaboy, D. Schmool, and J. M. Grenèche, Phys. Rev. B **81**, 094418 (2010).
[36] E. C. Stoner and E. P. Wohlfarth, Philos. Trans. R. Soc. London **240**, 599 (1948); IEEE Trans. Magn. **27**, 3475 (1991).
[37] D. Kirk, A. Kohn, K. B. Borisenko, C. Lang, J. Schmalhorst, G. Reiss, and D. J. H. Cockayne, Phys. Rev. B **79**, 014203 (2009).
[38] S. Cardoso, C. Cavaco, R. Ferreira, L. Pereira, M. Rickart, P. P. Freitas, N. Franco, J. Gouveia, and N. P. Barradas, J. Appl. Phys. **97**, 10C916 (2005).
[39] W. F. Shen, B. D. Schrag, A. Girdhar, M. J. Carter, H. Sang, and G. Xiao, Phys. Rev. B **79**, 014418 (2009).
[40] P. Wisniowski, J. M. Almeida, S. Cardoso, N. P. Barradas, and P. P. Freitas, J. Appl. Phys. **103**, 07A910 (2008).
[41] J. Ventura, J. M. Teixeira, J. P. Araujo, J. B. Sousa, P. Wisniowski, and P. P. Freitas, Phys. Rev. B **78**, 024403 (2008).
[42] J. M. Teixeira, J. Ventura, R. Fermento, J. P. Araujo, J. B. Sousa, P. Wisniowski, and P. P. Freitas, J. Phys. D **42**, 105407 (2009).
[43] J. M. Teixeira, J. Ventura, F. Carpinteiro, J. P. Araujo, J. B. Sousa, P. Wisniowski, and P. P. Freitas, J. Appl. Phys. **106**, 073707 (2009).
[44] J. Mathon and S. B. Ahmad, Phys. Rev. B **37**, 660 (1988).
[45] D. Mauri, D. Scholl, H. C. Siegmann, and E. Kay, Phys. Rev. Lett. **61**, 758 (1988).
[46] W. Kipferl, M. Sperl, T. Hagler, R. Meier, and G. Bayreuther, J. Appl. Phys. **97**, 10B313 (2005).
[47] W. Kipferl, M. Dumm, M. Rahm, and G. Bayreuther, J. Appl. Phys. **93**, 7601 (2003).
[48] M. Bowen, V. Cros, F. Petroff, A. Fert, C. Martinez Boubeta, J. L. Costa-Krämer, J. V. Anguita, A. Cebollada, F. Briones, J. M. de Teresa, L. Morellón, M. R. Ibarra, F. Güell, F. Peiró, and A. Cornet, Appl. Phys. Lett. **79**, 1655 (2001).
[49] Y. Xu, D. Ephron, and M. R. Beasley, Phys. Rev. B **52**, 2843 (1995).
[50] Y. Lu, M. Tran, H. Jaffrès, P. Seneor, C. Deranlot, F. Petroff, J-M. George, B. Lépine, S. Ababou, and G. Jézéquel, Phys. Rev. Lett. **102**, 176801 (2009).
[51] F. Guinea, Phys. Rev. B **58**, 9212 (1998).